Figures and figure supplements

Applying 3D correlative structured illumination microscopy and X-ray tomography to characterise herpes simplex virus-1 morphogenesis

Kamal L Nahas *et al*.

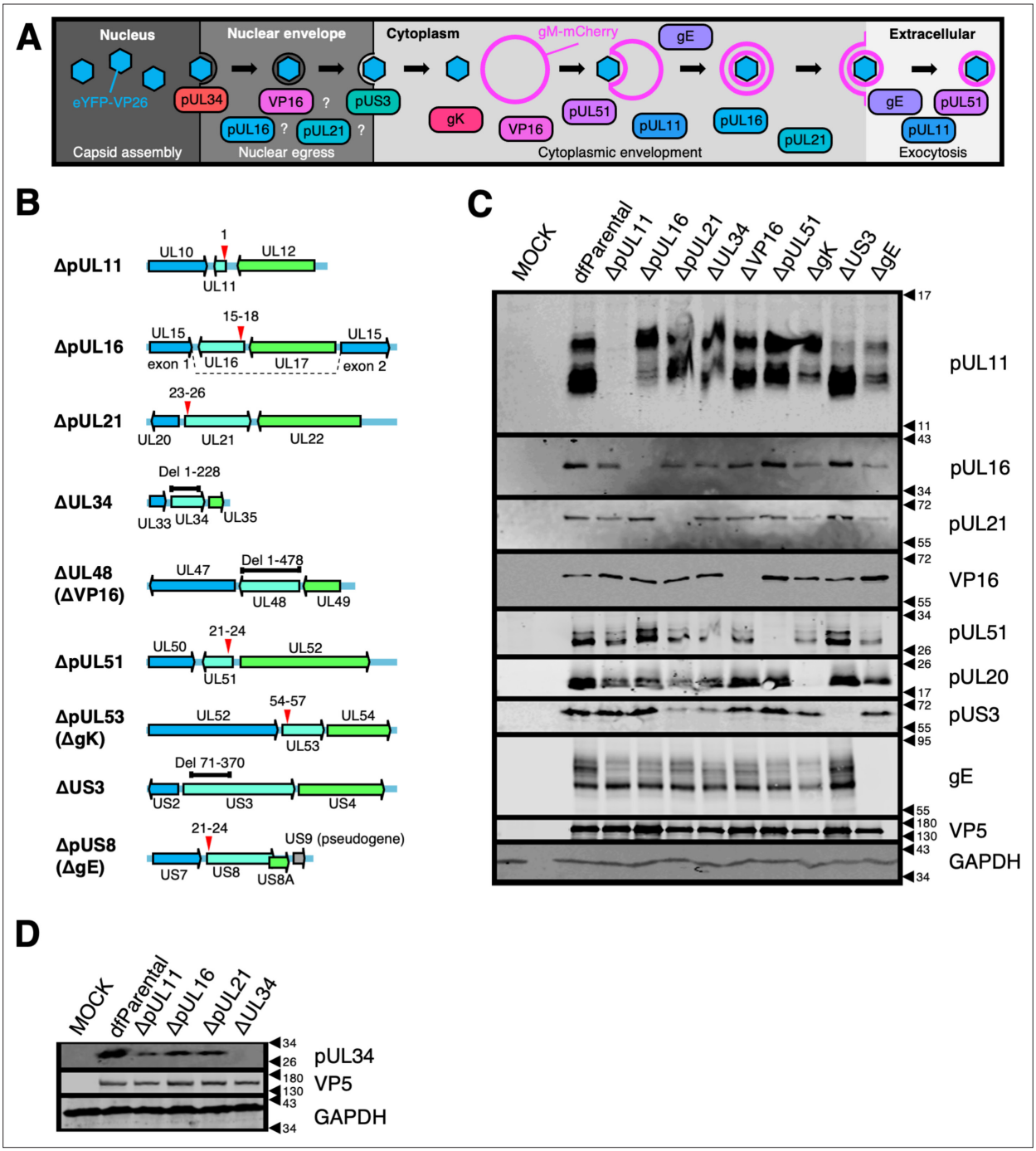

Figure 1. Characterisation of HSV-1 mutants. (**A**) Schematic of HSV-1 assembly with the proposed roles of viral proteins at different stages. Question marks denote that the role of the corresponding protein at that stage of HSV-1 assembly remains uncertain. Mutants with stop codons are named Δ+protein name (e.g. ΔpUL11), whereas mutants with sequence deletions are named Δ+ gene name (e.g. ΔUL34). Unique long (UL) and unique short (US) names are used except for proteins more commonly known by another name (i.e. ΔVP16, ΔgK, and ΔgE). (**B**) Schematic of recombinant viruses generated. Deletions (black bars) or stop codons (red arrows) were introduced into genes of interest (cyan) to prevent protein expression. Numbering refers to the amino acid residues of the corresponding protein. Flanking genes (blue and green) and pseudogene (mutated US9; grey) ***Negatsch et al., 2011*** in HSV-1 strain KOS are indicated. (**C–D**) Absence of protein expression was confirmed by immunoblotting infected Vero cell lysates with VP5 and GAPDH as viral and cellular loading controls, respectively. Due to the unavailability of an antibody that recognises gK, immunoblotting of pUL20 was used as an indicator of loss of gK expression since stable expression of gK and pUL20 relies on the presence of each other (***Foster et al., 2003***).

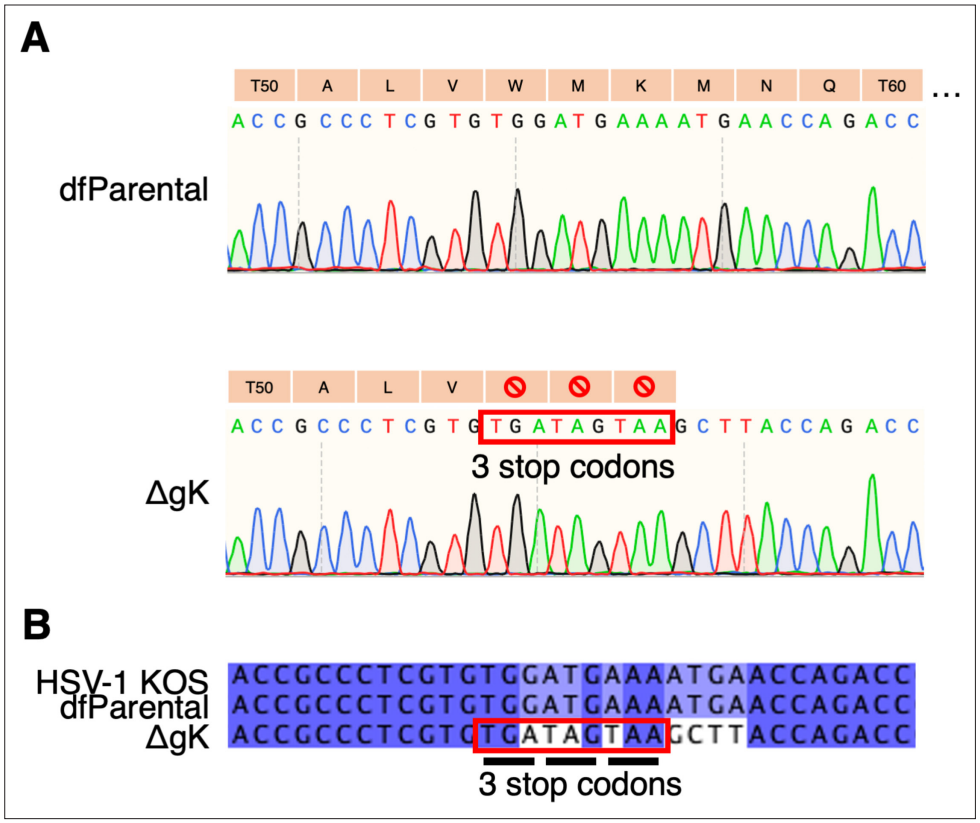

Figure 1—figure supplement 1. Sequence alignment of UL53 gene in ΔgK and dfParental HSV-1. (**A**) Sanger sequencing confirmed the presence of the three in-frame stop codons in the UL53 gene (encoding gK) of the ΔgK virus. Translated amino acid sequences are shown. (**B**) UL53 sequences from ΔgK and dfParental HSV-1 were aligned with the UL53 sequence of the KOS genome (GenBank accession number NC_001806) (***Macdonald et al., 2012***).

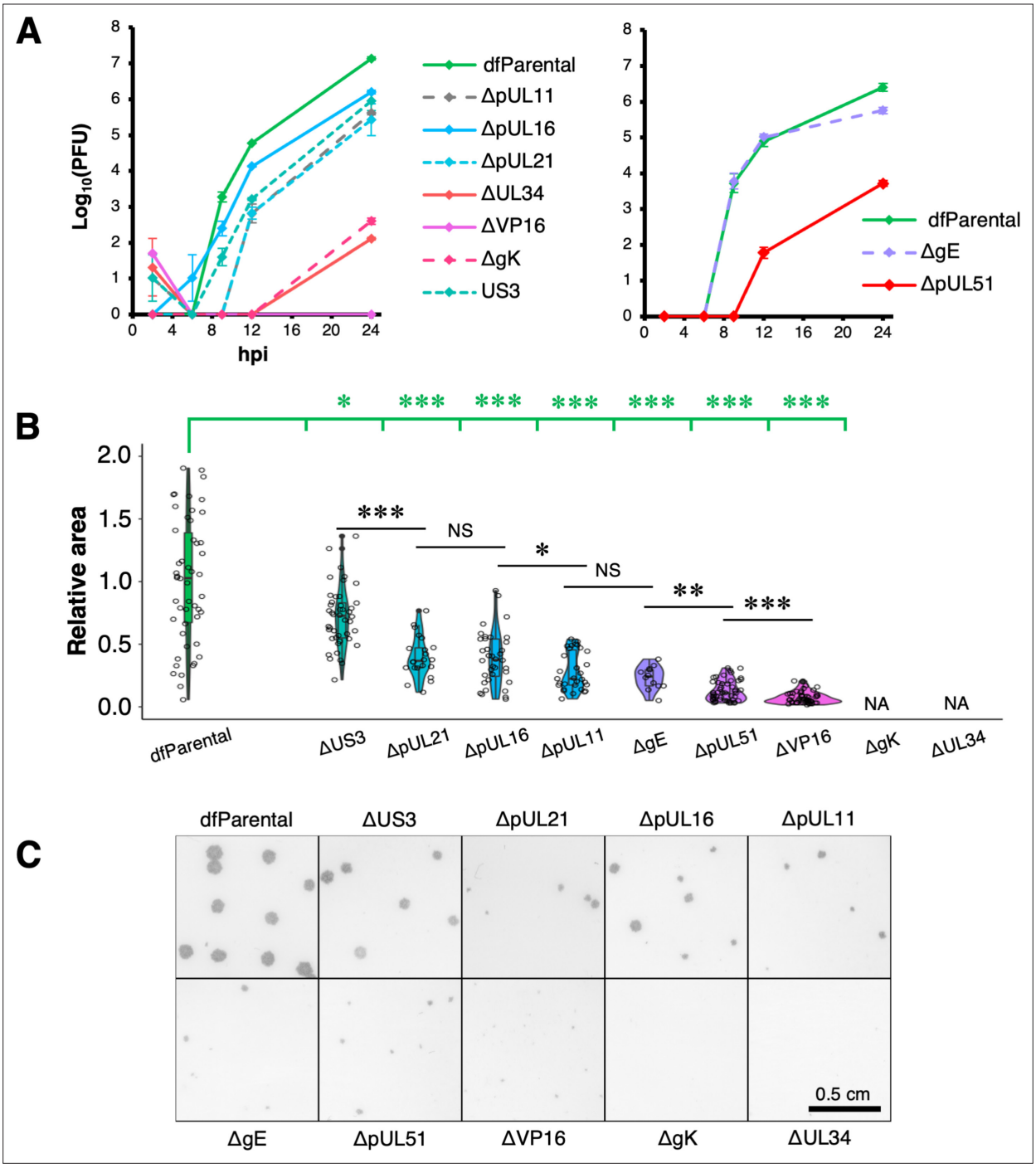

Figure 2. Replication kinetics and plaque assays of HSV-1 mutants. (**A**) Single-step replication curves on U2OS cells infected at MOI = 2 with virus. dfParental refers to eYFP-VP26 & gM-mCherry KOS used as a parental strain. U2OS cells were infected at MOI = 2 with virus over a 24 hr period and were treated with citric acid at the 1 hr timepoint to deactivate residual input virus. Titrations were performed on parental or complementing Vero cells. Two technical repeats were measured for each timepoint, and the data are representative of two biological replicates (***Figure 2—figure supplement 1***). Error bars show mean ± range. (**B**) 72 hr plaques were immunostained for gD using an antibody conjugated to horseradish peroxidase and were subsequently stained with DAB. Plaque area (pixels) were measured by applying thresholds to intensity using Fiji and quantifying the number of pixels in each plaque from binary masks (***Rueden et al., 2017***; ***Schindelin et al., 2012***). Measurements were taken from a range of plaques for each recombinant virus: dfParental (N=50), ΔUS3 (N=44), ΔpUL21 (N=22), ΔpUL16 (N=36), ΔpUL11 (N=31), ΔgE (N=12), ΔpUL51 (N=50), and ΔVP16 (N=50). Given the skewed distributions, non-parametric Mann-Whitney *U* tests were used to assess the significance of differences. P-value thresholds: <0.05 (*), <0.005 (**), and <0.0005 (***). NS, no significance; NA, not applicable. (**C**) Images of 72 hr plaques from dfParental and mutants.

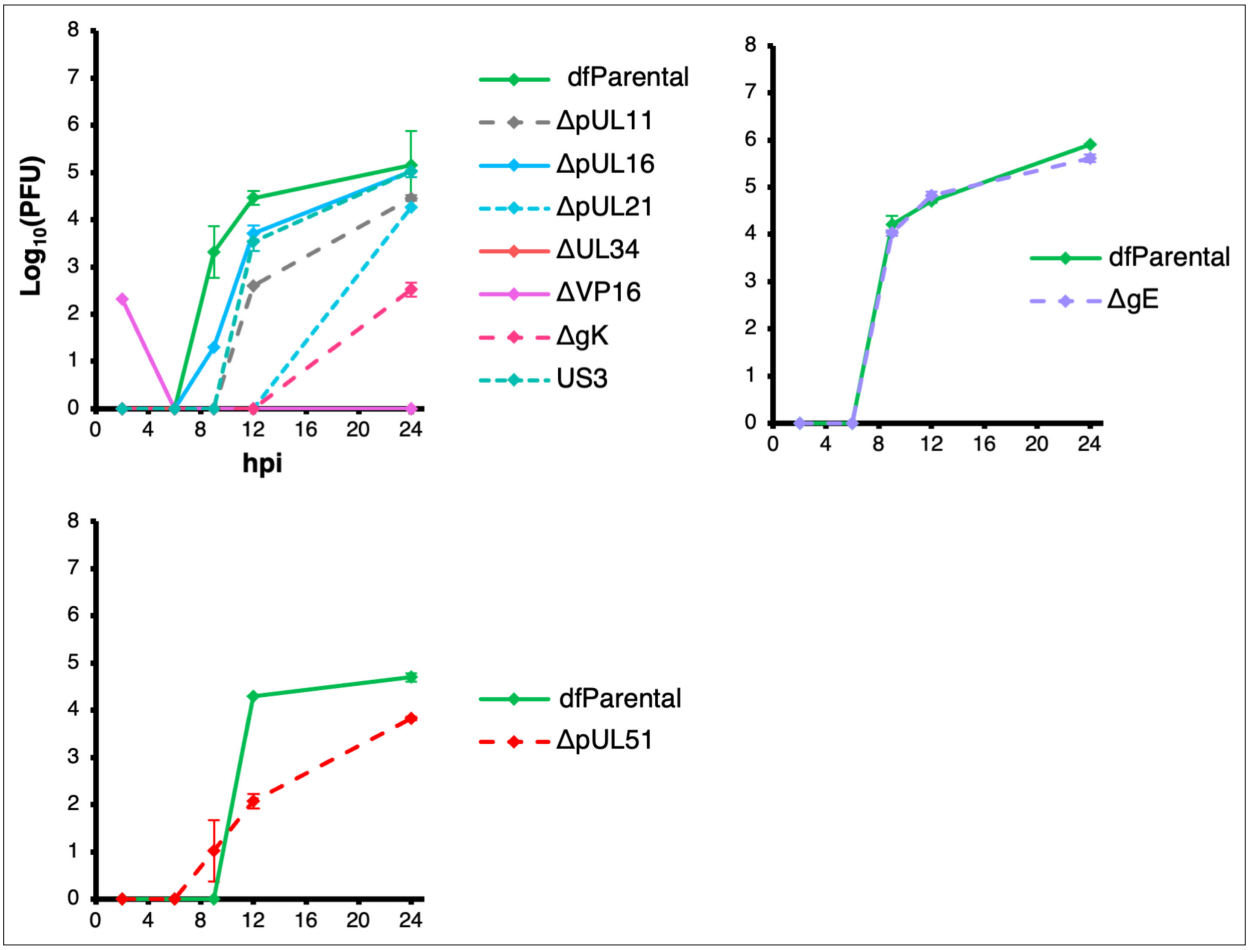

Figure 2—figure supplement 1. Additional replicate for single-step replication kinetics of mutant and dfParental HSV-1. Single-step replication curves on U2OS cells infected at MOI = 2 with virus. dfParental refers to the parental eYFP-VP26 & gM-mCherry KOS strain. U2OS cells were infected at MOI = 2 with virus over a 24 hr period and were treated with citric acid at the 1 hr timepoint to deactivate extracellular viruses. Titrations were performed on parental or complementing Vero cells. Two technical repeats were measured for each timepoint, and the data are representative of two biological replicates (***Figure 2***). Error bars show mean ± range.

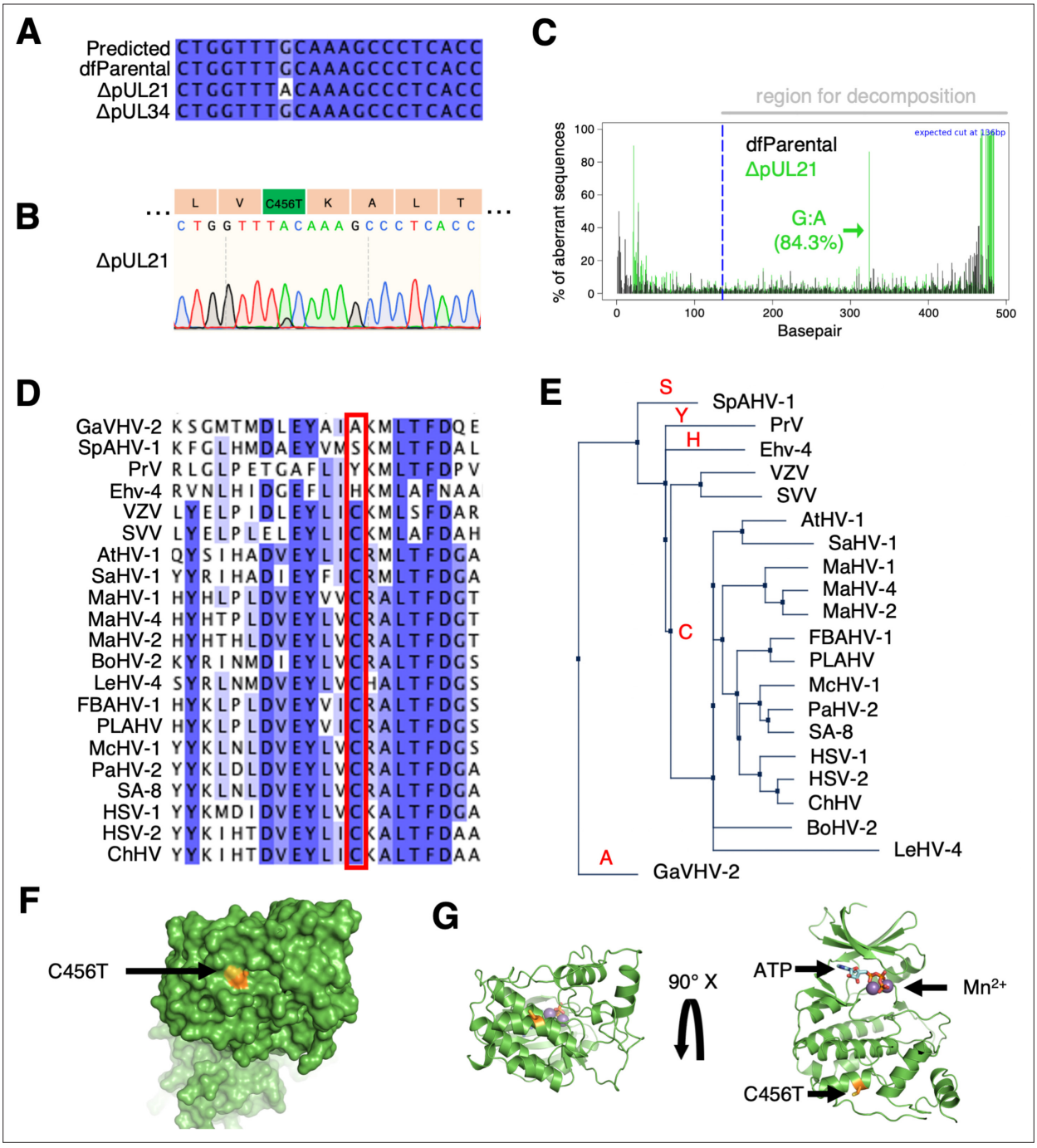

Figure 2—figure supplement 2. Sequence alignment of US3 in recombinant and dfParental viruses. (**A**) Sanger sequencing of the US3 gene revealed a guanine to adenine mutation at base pair 1367 in the ΔpUL21 virus but not the ΔUL34 virus. Sequencing results were compared against the KOS genome (HSV-1 KOS; GenBank accession number NC_001806) (***Macdonald et al., 2012***). (**B**) This mutation resulted in a C456T substitution in pUS3. (**C**) Tracking of Indels by Decomposition (TIDE) (***Brinkman et al., 2014***) analysis was performed to identify prevalent base pair changes in the US3 gene of the ΔpUL21 virus. The mutation at base pair 1367 was 84.3% prevalent and no other prevalent mutations were identified. (**D**) pUS3 orthologues from 21 alphaherpesviruses were aligned to assess conservation of amino acid residue in question. Only four species contained different residues at this position. Species aligned (abbreviation, sequence ID): Gallus alphaherpesvirus 2 (GaVHV-2, GenBank: ACF94893.1), Spheniscid alphaherpesvirus 1 (SpAHV-1, GenBank: SCL76985.1), Pseudorabies virus (PrV, UniProtKB/Swiss-Prot: P24381.2), Equine herpesvirus 4 (Ehv-4, GenBank: BAV93592.1), Varicella Zoster Virus (VZV, NCBI Reference Sequence: NP_040188.1), Simian Varicella Virus (SVV, UniProtKB/Swiss-Prot: Q04543.1), Ateline herpesvirus 1 (AtHV-1, NCBI Reference Sequence: YP_009361942.1), Saimiriine herpesvirus 1 (SaHV-1, NCBI Reference Sequence: YP_003933845.1), Macropodid alphaherpesvirus 1 (MaHV-1, NCBI Reference Sequence: YP_009227221.1), Macropodid alphaherpesvirus 4 (MaHV-4, NCBI Reference Sequence: YP_010801716.1), Macropodid alphaherpesvirus 2 (MaHV-2, NCBI Reference Sequence: YP_010798801.1), Bovine alphaherpesvirus 2 (BoHV-2, NCBI

Figure 2—figure supplement 2 continued on next page

Figure 2—figure supplement 2 continued

Reference Sequence: YP_010798781.1), Leporid alphaherpesvirus 4 (LeHV-4, NCBI Reference Sequence: YP_009230196.1), Fruit bat alphaherpesvirus-1 (FBAHV-1, NCBI Reference Sequence: YP_009042124.1), Pteropus lylei-associated alphaherpesvirus (PLAHV, NCBI Reference Sequence: YP_010801544.1), Macacine alphaherpesvirus 1 (McHV-1, NCBI Reference Sequence: YP_010797361.1), Papiine alphaherpesvirus 2 (PaHV-2, GenBank: AHM96184.1), Herpes simian agent 8 (SA-8, NCBI Reference Sequence: YP_164505.1), Herpes simplex virus 1 (HSV-1, GenBank: AKG59533.1), Herpes simplex virus 2 (HSV-2, UniProtKB/Swiss-Prot: P13287.1), Chimpanzee herpesvirus (ChHV, NCBI Reference Sequence: YP_009011050.1) (**E**) A neighbour-joining tree of the aligned sequences revealed the pUS3 orthologues containing the conserved C residue were more similar to each other than to the orthologues containing the A, H, S, or Y residues. (**F**) A model of pUS3 was superposed onto the structure of Protein Kinase A[33], and a surface map revealed the mutated residue is exposed. (**G**) A ribbon model of the structure in F shows that the mutated residue is not located near the kinase active site, which is indicated by the ATP and metal ions (***Thompson et al., 2009***).

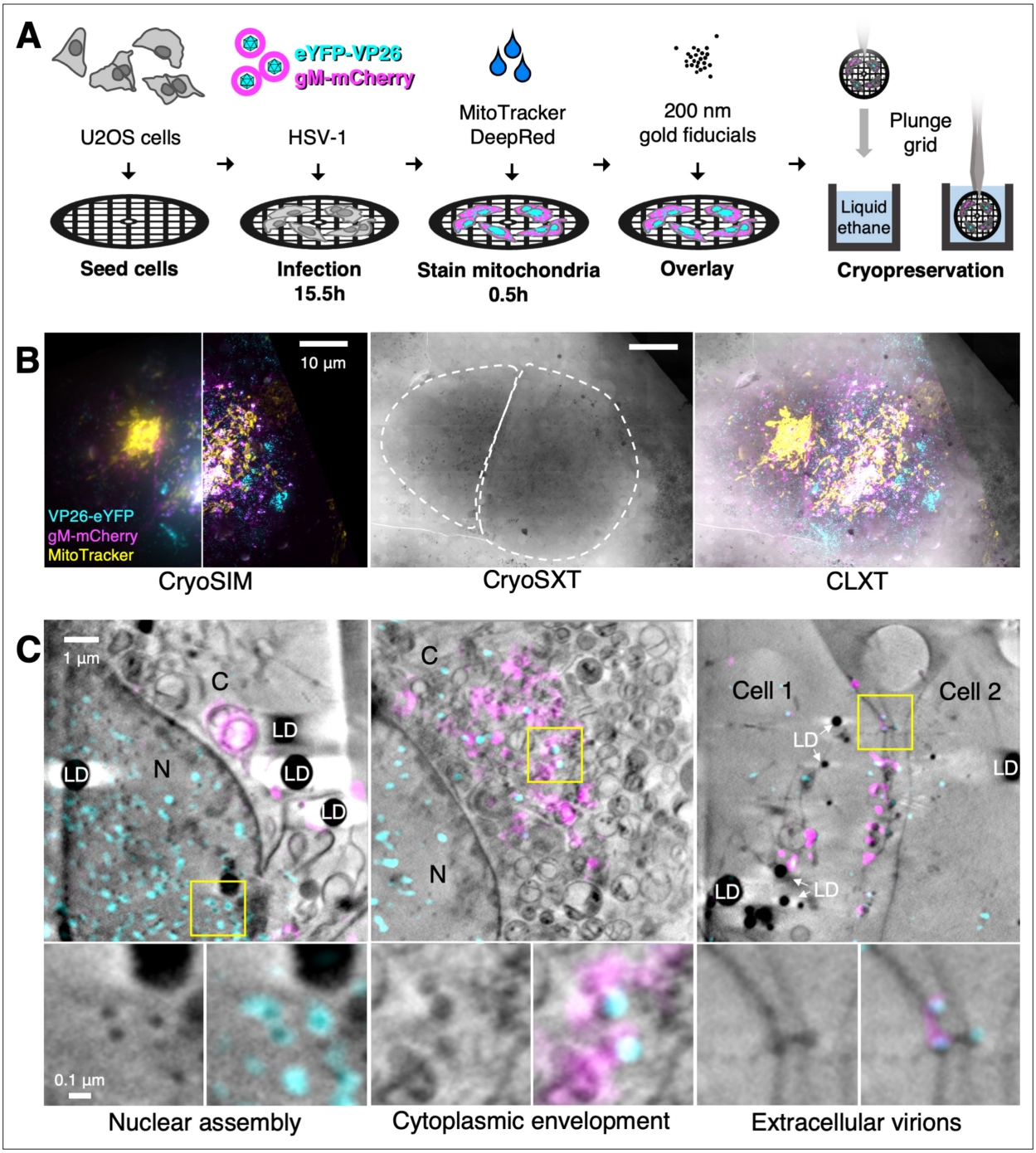

Figure 3. Correlative imaging workflow to study dfParental HSV-1 assembly. U2OS cells were infected at MOI = 2 with dfParental HSV-1 for 16 hr. (**A**) A schematic of sample preparation. U2OS cells were seeded on 3 mm TEM grids, infected with the dfParental virus for 15.5 hr, mitochondria were stained with MitoTracker Deep Red (Thermo Fisher Scientific) for 0.5 hr, and 200 nm gold fiducials were overlayed onto the cells immediately before cryopreservation by plunge cryocooling in liquid ethane. (**B**) Cryopreserved samples were imaged first by cryoSIM and subsequently by cryo-soft-X-ray tomography (cryoSXT). The left and right sides of the cryoSIM image show the data at conventional resolution (left) and after it was super-resolved in a cryoSIM reconstruction (right). CryoSIM fluorescence was then correlated onto the CryoSXT datasets by comparing the MitoTracker stain with mitochondria in the tomograms. Scale bars = 10 µm. (**C**) CLXT was used to identify virus assembly intermediates in U2OS cells infected with the dfParental tagged virus. eYFP-VP26^{+}/gM-mCherry^{-} particles were identified in the nucleus (N). eYFP-VP26^{+}/gM-mCherry^{+} particles were identified in the cytoplasm (C) where cytoplasmic envelopment occurs. eYFP-VP26^{+}/gM-mCherry^{+} particles were also identified in spaces between cells. LD = lipid droplets.

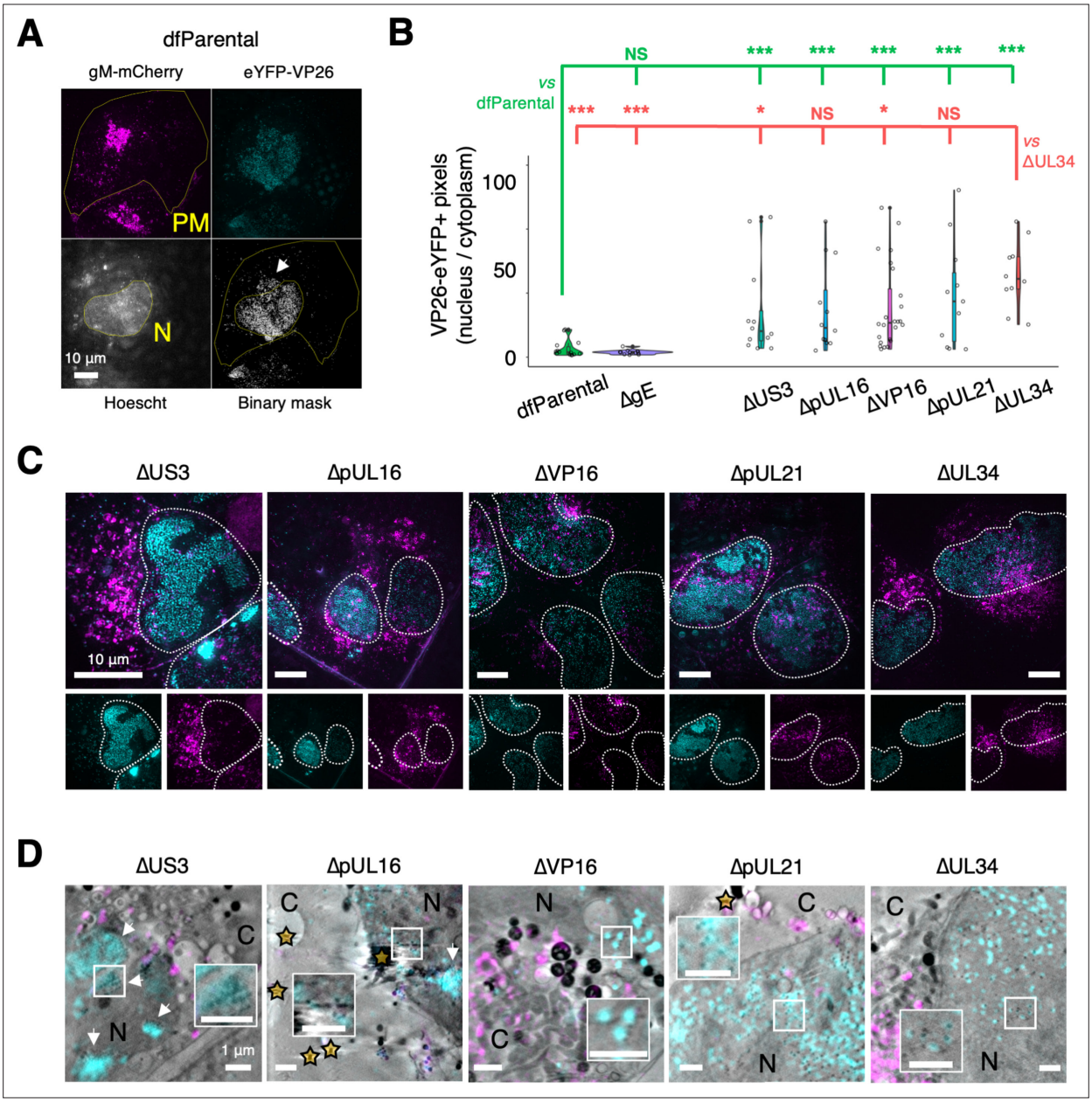

Figure 4. CryoSIM and correlative light X-ray tomography (CLXT) of nuclear egress attenuation. U2OS cells were infected at MOI = 2 with indicated viruses for 16 hr. Mutant-specific defects in nuclear egress were investigated using maximum Z projections of cryoSIM data. (**A**) eYFP-VP26 fluorescence was captured in punctate form, representing individual virus particles or clusters. Digitally saturated gM-mCherry was used to delineate the plasma membrane (PM) of infected cells and the Hoechst stain was used to delineate the nucleus (N). A binary mask of eYFP-VP26 fluorescence was generated to include capsids or capsid clusters and filter out background or noise. The arrow indicates fluorescent viral proteins in the cytoplasm. Scale bars = 10 µm. (**B**) The number of pixels containing capsids or capsid clusters in the nucleus and cytoplasm was counted using the plasma membrane and nucleus borders. The nuclear:cytoplasmic (N:C) ratio of capsids was lowest for the dfParental-infected cells and the ΔgE-infected cells (negative control) and was significantly higher for the other mutants. Owing to the skewed distributions, the significance of differences was assessed using non-parametric Mann-Whitney *U* tests between dfParental (N=14) (green statistics) or ΔUL34 (N=10) (red statistics) and other viruses, specifically ΔpUL16 (N=13), ΔpUL21 (N=11), ΔUS3 (N=13), ΔVP16 (N=24), and ΔgE (N=12). NS; no significance. P-value thresholds: <0.05 (*), <0.005 (**), and <0.0005 (***). (**C**) Representative viral fluorescence cryoSIM data for the mutants. Note that the ΔUS3 example was reused in ***Figure 5C***. Scale bars = 10 µm. (**D**) Correlative cryoSIM and cryo-soft-X-ray tomography (cryoSXT) data for the mutants. Inset images show correlated nuclear capsids at twice the magnification. Scale bars = 1 µm. Nuclear clusters of capsids (known as assemblons ***Ward et al., 1996***; ***Lee et al., 2006a***) are visible in the ΔUS3 and ΔpUL16 datasets (arrows). Stars indicate gold fiducials. C, cytoplasm.

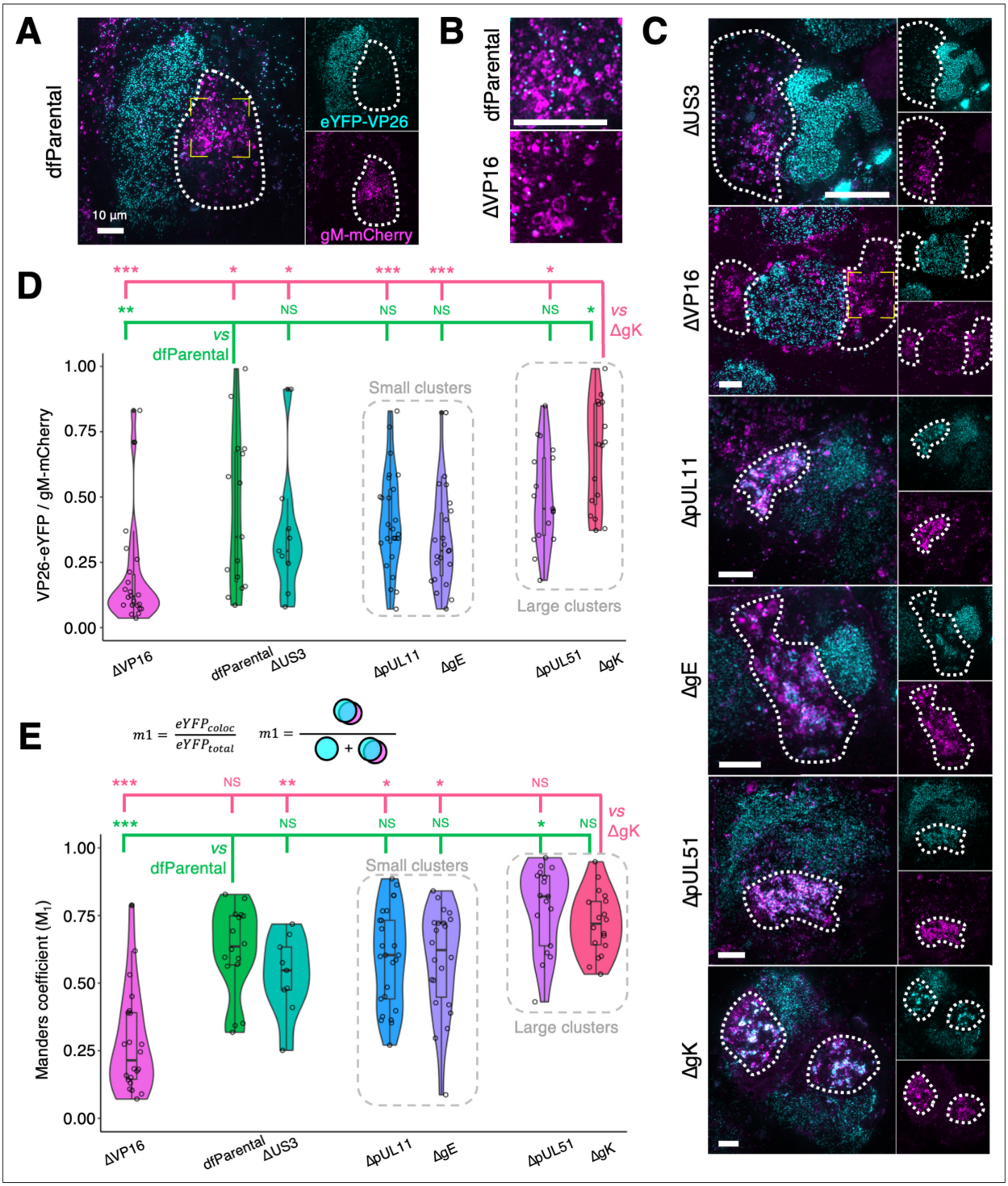

Figure 5. Cytoplasmic clustering of virus particles imaged using cryoSIM. U2OS cells were infected at MOI = 2 with indicated viruses for 16 hr. Cytoplasmic clustering of mutants was investigated using maximum Z projections of cryoSIM data. Scale bars = 10 µm. (**A**) gM-mCherry fluorescence was used to determine the cytoplasmic region in which virus assembly occurs, known as the juxtanuclear assembly compartment (JAC, dotted outline). The yellow corner markings denote the region of the dfParental virus-infected cell shown in **B**. (**B**) Cytoplasmic capsids at the JAC in ΔVP16-infected cells were less abundant and less closely associated with gM-mCherry$^+$ endomembranes compared with those of dfParental-infected cells. (**C**) Representative images of JACs (dotted outline) for mutants. The JACs for the ΔUS3 virus were similar to those of the dfParental. ΔVP16 produced few cytoplasmic virus particles, ΔpUL11 and ΔgE produced small cytoplasmic clusters of capsids, and ΔpUL51 and ΔgK produced large cytoplasmic capsid clusters. The yellow corner markings denote the region of the ΔVP16 virus-infected cell shown in **B**. Note that the ΔUS3 example was reused in ***Figure 4C***. (**D**) Thresholding of eYFP-VP26 and gM-mCherry fluorescence to filter out noise and background was performed and binary masks were

Figure 5 continued on next page

Figure 5 continued

produced. The ratio of eYFP-VP26^{+} pixels to gM-mCherry^{+} pixels at the JACs was reported. Data from the ΔUS3 virus were included as a negative control for attenuation in cytoplasmic virion assembly. (**E**) Manders coefficients (M_1) were measured for each virus and represent the amount of eYFP-VP26 fluorescence that colocalises with gM-mCherry ($eYFP_{coloc}$) as a proportion of all eYFP-VP26 fluorescence at the JAC ($eYFP_{total}$). M_1 values were markedly lower for the ΔVP16 virus than other viruses. M_2 values are shown in ***Figure 5—figure supplement 1***. Mann-Whitney *U* tests were performed to assess significance of differences between dfParental (N=16) (green statistics) or ΔgK (N=18) (pink statistics) and other viruses, specifically ΔUS3 (N=9), ΔVP16 (N=22), ΔgE (N=23), ΔpUL11 (N=25), and ΔpUL51 (N=17). P-value thresholds: <0.05 (*), <0.005 (**), and <0.0005 (***). NS, no significance.

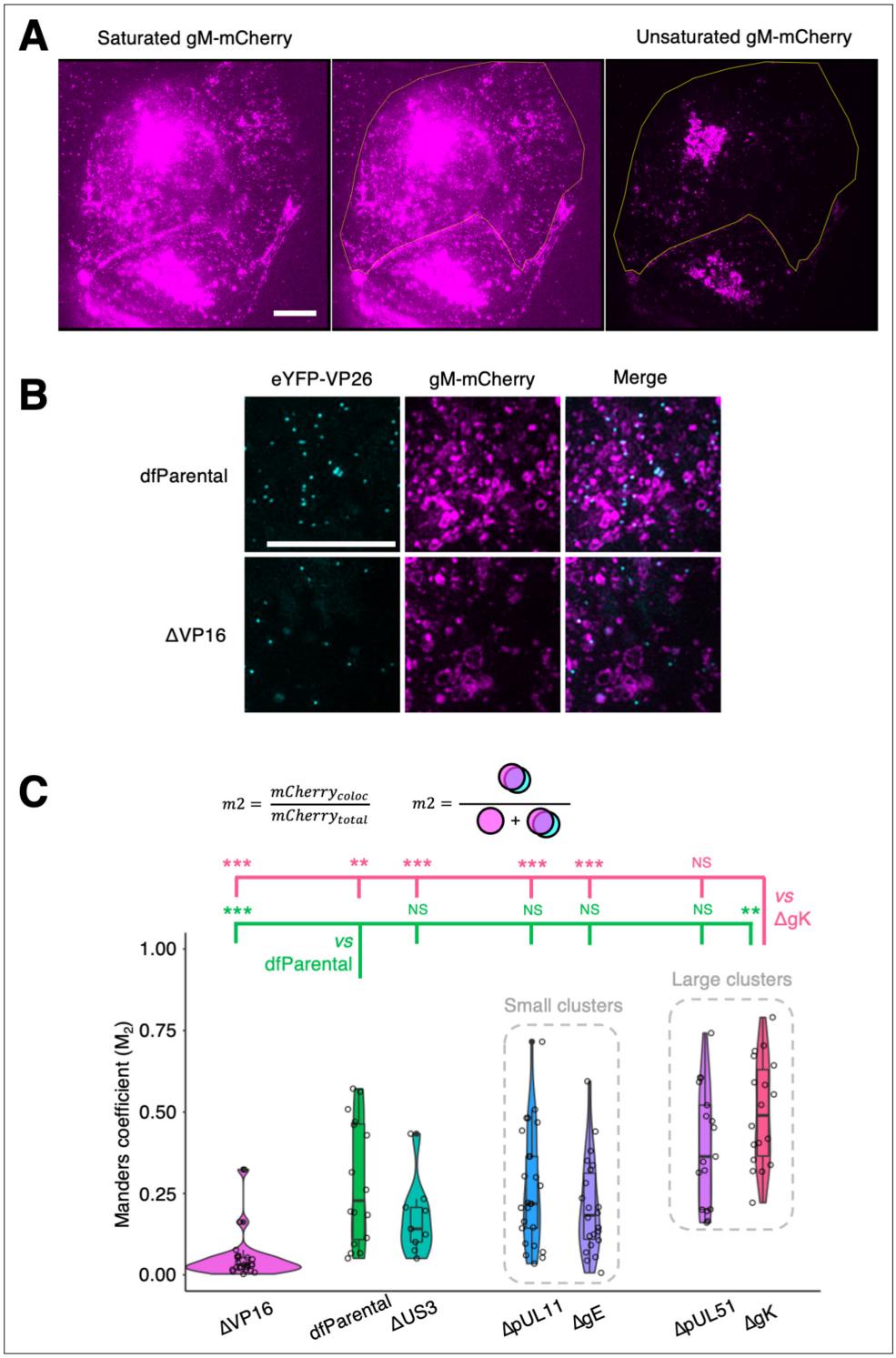

Figure 5—figure supplement 1. Association of gM-mCherry⁺ endomembranes with capsids. U2OS cells were infected at MOI = 2 with indicated viruses for 16 hr. Scale bars = 10 µm. (**A**) Saturation of gM-mCherry⁺ endomembranes was used to delineate the borders of the cytoplasm (yellow silhouette). This example taken from ***Figure 4A*** shows a cell infected with the dfParental virus. (**B**) Individual and combined channels for data in ***Figure 5B*** showcasing the reduced association of ΔVP16 capsids with gM-Cherry⁺ endomembranes compared with the dfParental virus. (**C**) Manders coefficients (M_2) were measured for each virus and represent the amount of gM-mCherry fluorescence that colocalised with eYFP-VP26 ($mCherry_{coloc}$) as a proportion of total gM-mCherry fluorescence at the JAC ($mCherry_{total}$). M_2 values were markedly lower for the ΔVP16 virus than other viruses. Data

Figure 5—figure supplement 1 continued on next page

Figure 5—figure supplement 1 continued

from the ΔUS3 virus were included as negative control for attenuation in cytoplasmic virion assembly. Mann-Whitney *U* tests were performed to assess significance of differences between dfParental (N=16) (green statistics) or ΔgK (N=18) (pink statistics) and other viruses, specifically ΔUS3 (N=9), ΔVP16 (N=22), ΔgE (N=23), ΔpUL11 (N=25), and ΔpUL51 (N=17). P-value thresholds: <0.05 (*), <0.005 (**), and <0.0005 (***). NS, no significance.

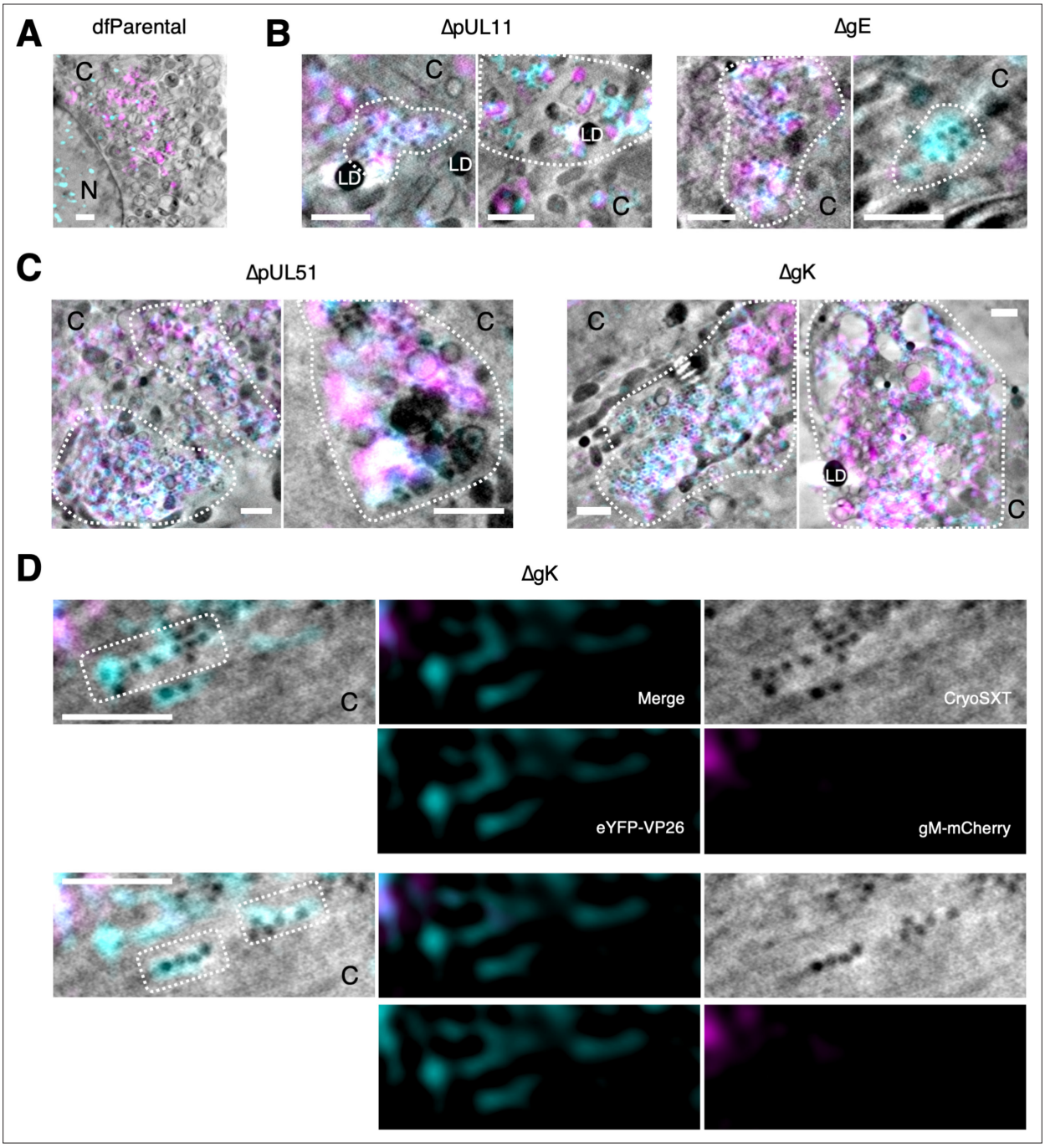

Figure 6. Correlative light X-ray tomography (CLXT) of cytoplasmic clusters of mutants. U2OS cells were infected at MOI = 2 with indicated viruses for 16 hr. (**A**) Individual envelopment events (arrows) as opposed to cytoplasmic clusters were observed for the dfParental virus. To aid visual comparison, this panel depicts the same data as shown in ***Figure 3C***. C, cytoplasm; N, nucleus. (**B**) Cells infected with ΔpUL11 or ΔgE viruses contained small clusters of capsids (outlined) in the juxtanuclear assembly compartment (JACs). (**C**) Cells infected with ΔpUL51 or ΔgK viruses contained large clusters of capsids (outlined) in the JACs. (**D**) Linear arrays of eYFP-VP26^{+}/gM-mCherry^{-} virus particles (outlined) were observed in the cytoplasm of a cell infected with ΔgK. Scale bars = 1 μm.

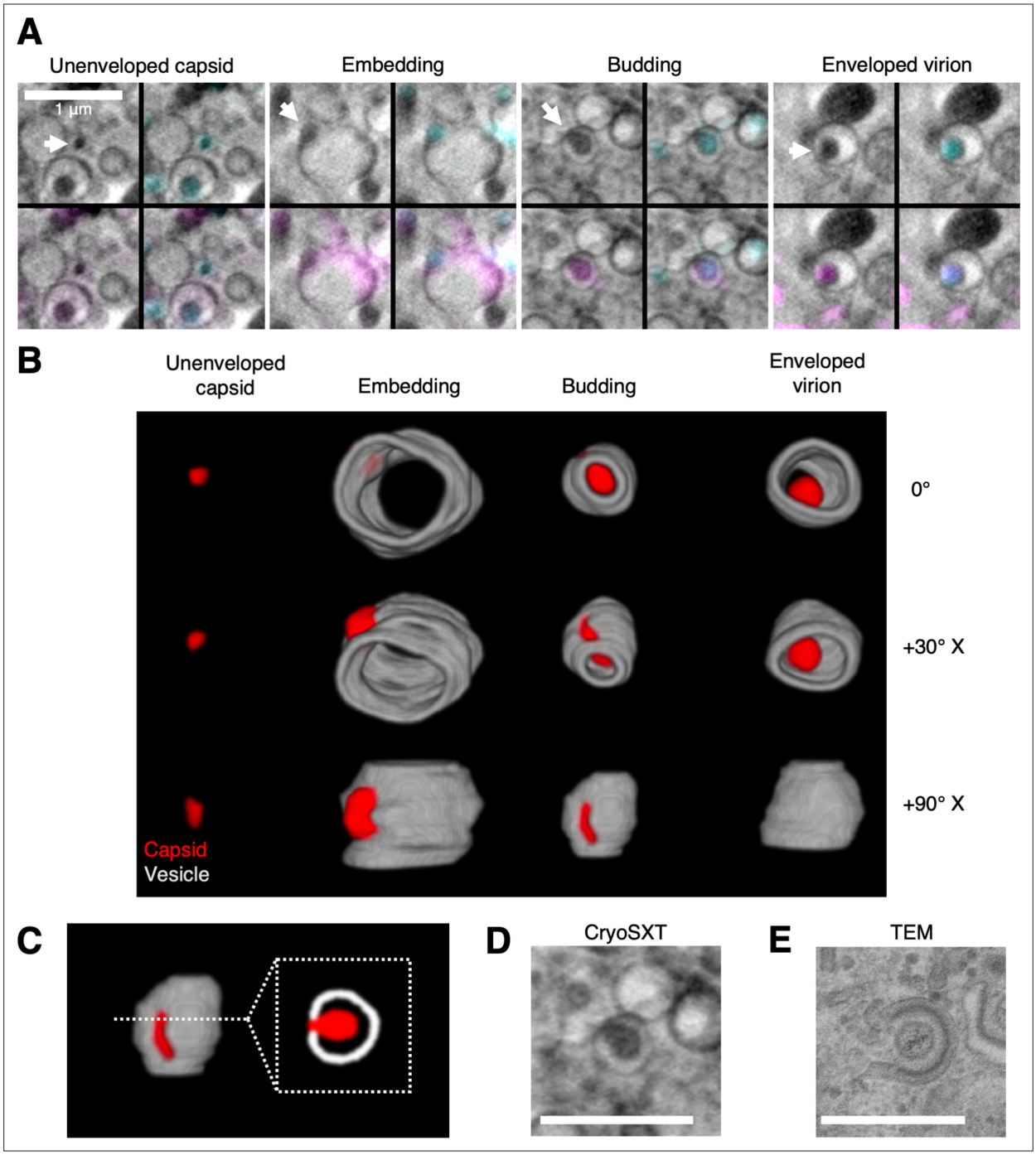

Figure 7. 3D Snapshots of the trajectory of ΔpUL51 HSV-1 envelopment within the cytoplasm. U2OS cells were infected at MOI = 2 with ΔpUL51 HSV-1 for 16 hr. (**A**) Correlative light X-ray tomography (CLXT) revealed multiple stages in the assembly of the ΔpUL51 virus (arrows). (**B**) 3D renderings of the assembly stages captured by CLXT in A at different rotations around the X-axis. The vesicles appear open-ended because the anterior and posterior faces lack sufficient contrast for reliable segmentation — a result of the X-ray tilt series spanning 120° rather than 180°. (**C**) Capsids can be seen budding into vesicles. A cross-section through the middle gives the appearance of a capsid being wrapped by a tubular membrane. (**D**) A 2D cryo-soft-X-ray tomography (CryoSXT) projection of an envelopment event. (**E**) A 2D TEM of an envelopment event from an HFF-hTERT cell infected with an untagged wild-type (WT) HSV-1 (KOS strain). Scale bars = 1 µm.

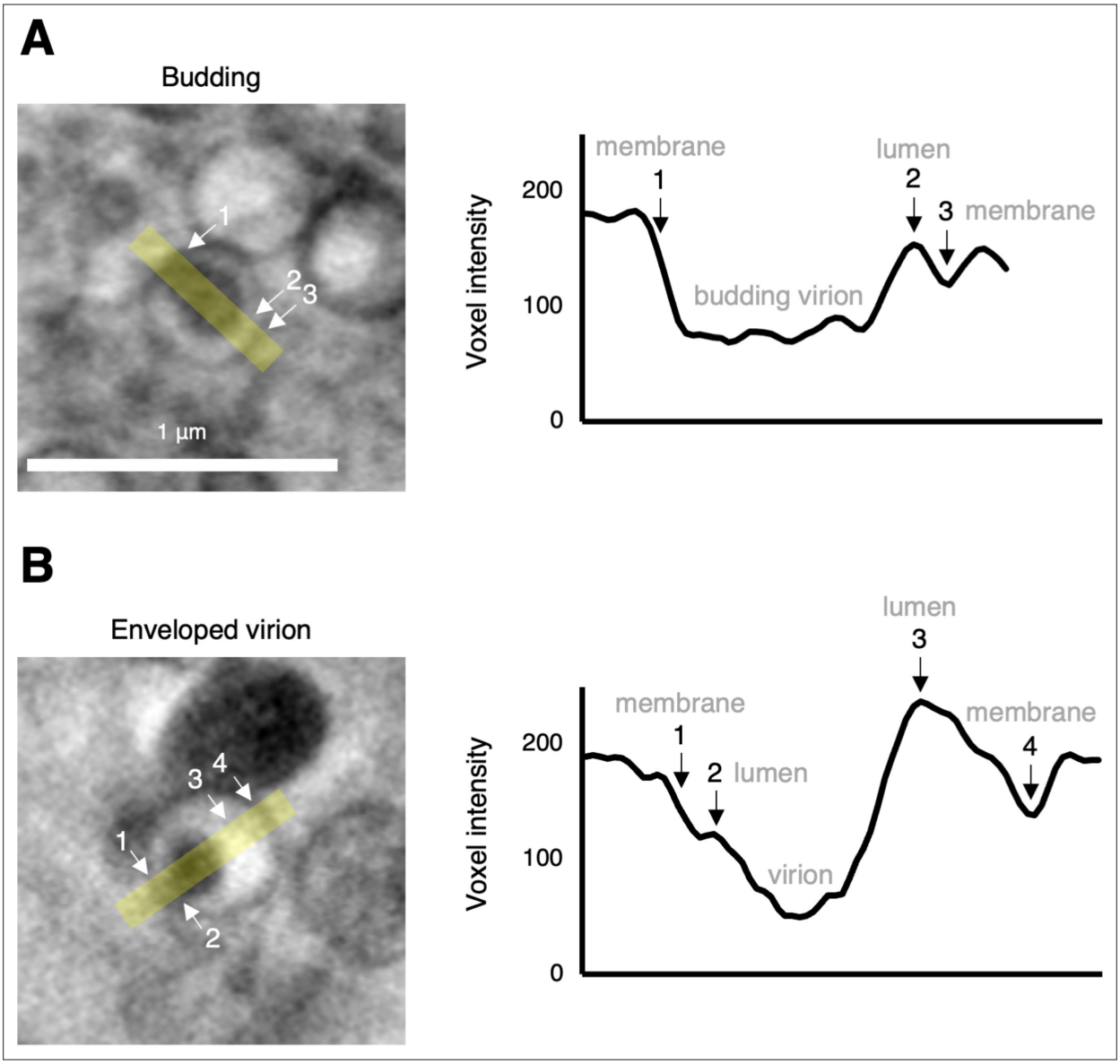

Figure 7—figure supplement 1. Full and partial envelopment intermediates distinguished based on voxel intensity. Using U2OS cells infected at MOI = 2 with the ΔpUL51 virus for 16 hr, cryo-soft-X-ray tomography (cryoSXT) captures (**A**) a virus particle budding into the lumen of a vesicle and (**B**) a fully enveloped virion within a vesicle. Voxel intensities were measured from the yellow stripes (width = 10 voxels) using Fiji, and notable features are numbered. The budding virion in **A** cannot be distinguished from the membrane, whereas the virion in **B** is separated from the membrane by a brighter lumen. Scale bars = 1 µm.

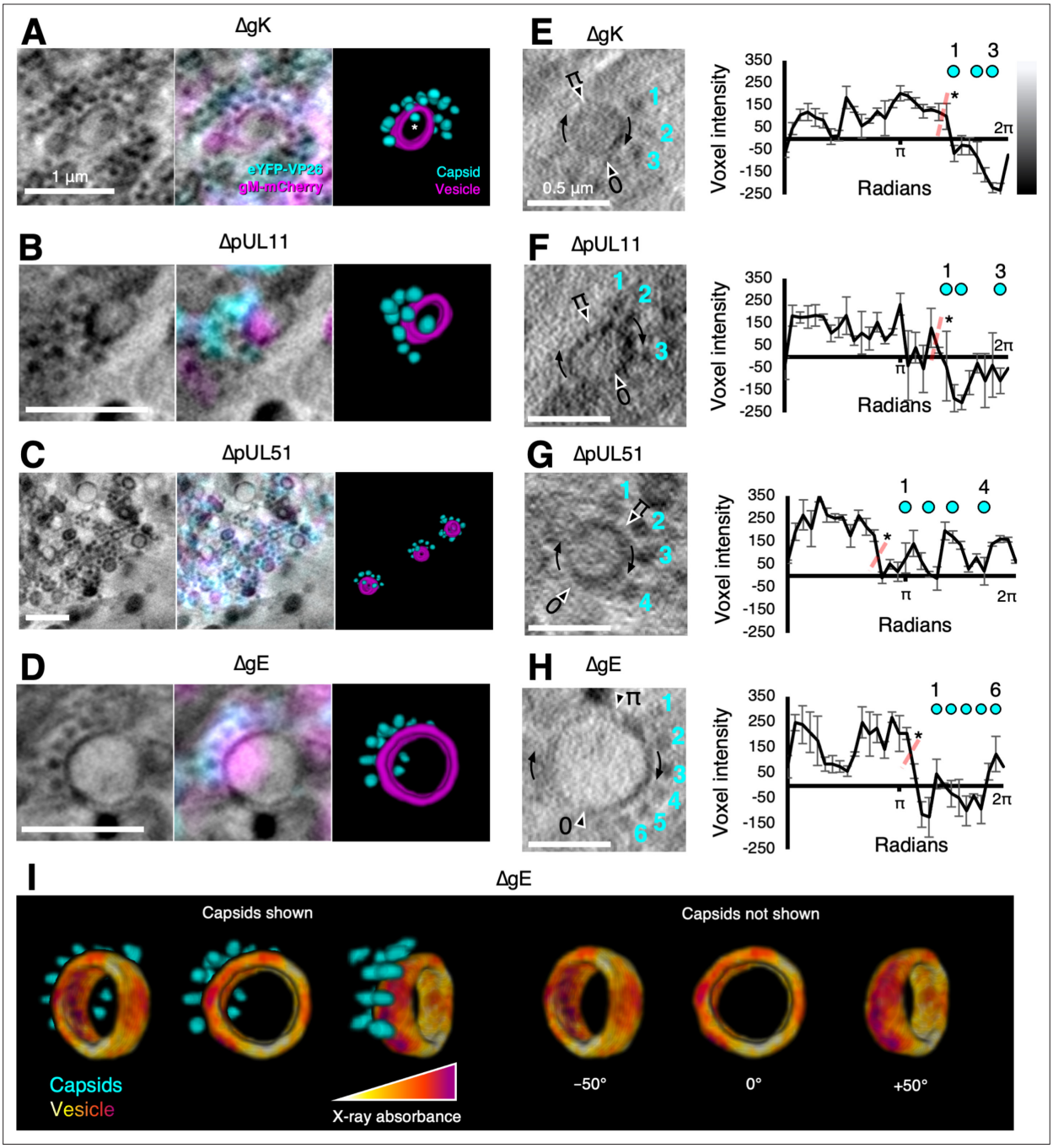

Figure 8. Mutants exhibit features of stalled envelopment. U2OS cells were infected at MOI = 2 with indicated viruses for 16 hr. (**A–D**) Arrays of unenveloped cytosolic capsids were observed near gM-mCherry-enriched vesicles for the indicated viruses. Vesicles were enriched in gM-mCherry at the pole nearest the capsid arrays. We interpret these features as capsids interacting with the appropriate target membranes but experiencing a delay or defect in budding. Some capsids appear to be located in the lumen of the vesicle (e.g. capsid marked with an asterisk (*) in **A**), but these are in fact external and located in front of or behind the open-ended segmentation of the vesicle. The vesicles appear open-ended because the X-ray tilt series spanned only 120°, causing the anterior and posterior faces to lack sufficient contrast for reliable segmentation. (**E–H**) For each indicated virus, the voxel intensity was measured at 30 points on the vesicles to provide a measure of the X-ray absorbing material present on the vesicle. Voxel intensities were plotted against the positions of the proximal capsids. Voxel intensities were measured from three projection planes spanning a depth of 30 nm and error bars show mean ± SD of these three planes. Two-tailed t-tests were performed to determine the significance of difference between the side of the vesicle nearest the capsids and the other side, as indicated by the dotted red line. Voxel intensity was lower on the side nearest the capsids, indicating this pole of the membrane contained a greater X-ray absorbing material. (**I**) A false-coloured heatmap of voxel intensity from the cryo-soft-X-ray tomography (cryoSXT) data was superimposed onto the vesicle segmentation from **D**. The vesicle is displayed at three angles with or without the proximal capsid arrays. The reciprocal of voxel intensity was used as a proxy for X-ray absorbance. The pole of the vesicle near the capsid arrays had greater X-ray absorption (red/purple) than the opposite pole (yellow/orange). Scale bars = 1 μm in **A–D** and 0.5 μm in **E–H**.

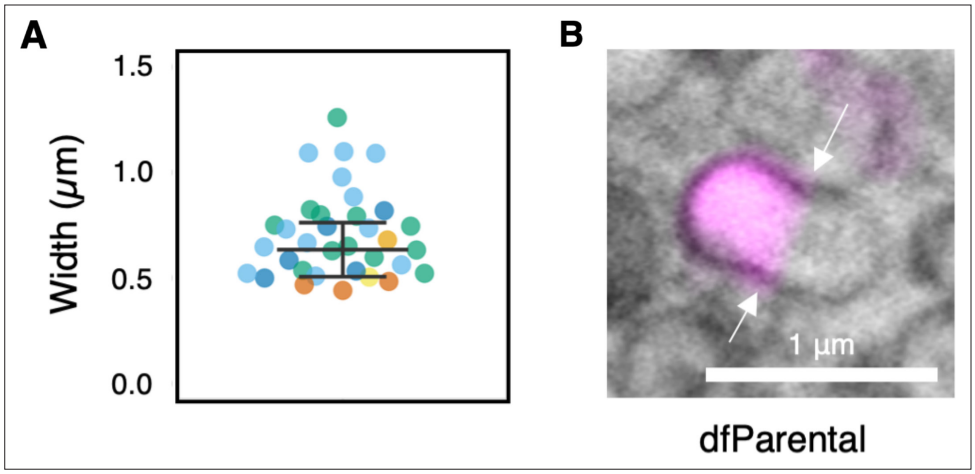

Figure 8—figure supplement 1. Features of gM-mCherry⁺ vesicles in infected cells. (**A**) Widths of vesicles associated with capsid arrays were measured using *Contour* (***Nahas et al., 2022b***) and are colour-coded by source tomogram. Error bars show mean ± SD (n=34). (**B**) Polarisation of gM-mCherry was also observed in dfParental-infected cells and membrane constrictions were visible (arrows), suggesting vesicle fission, fusion, or pressure imposed by microtubules. Scale bars = 1 μm.

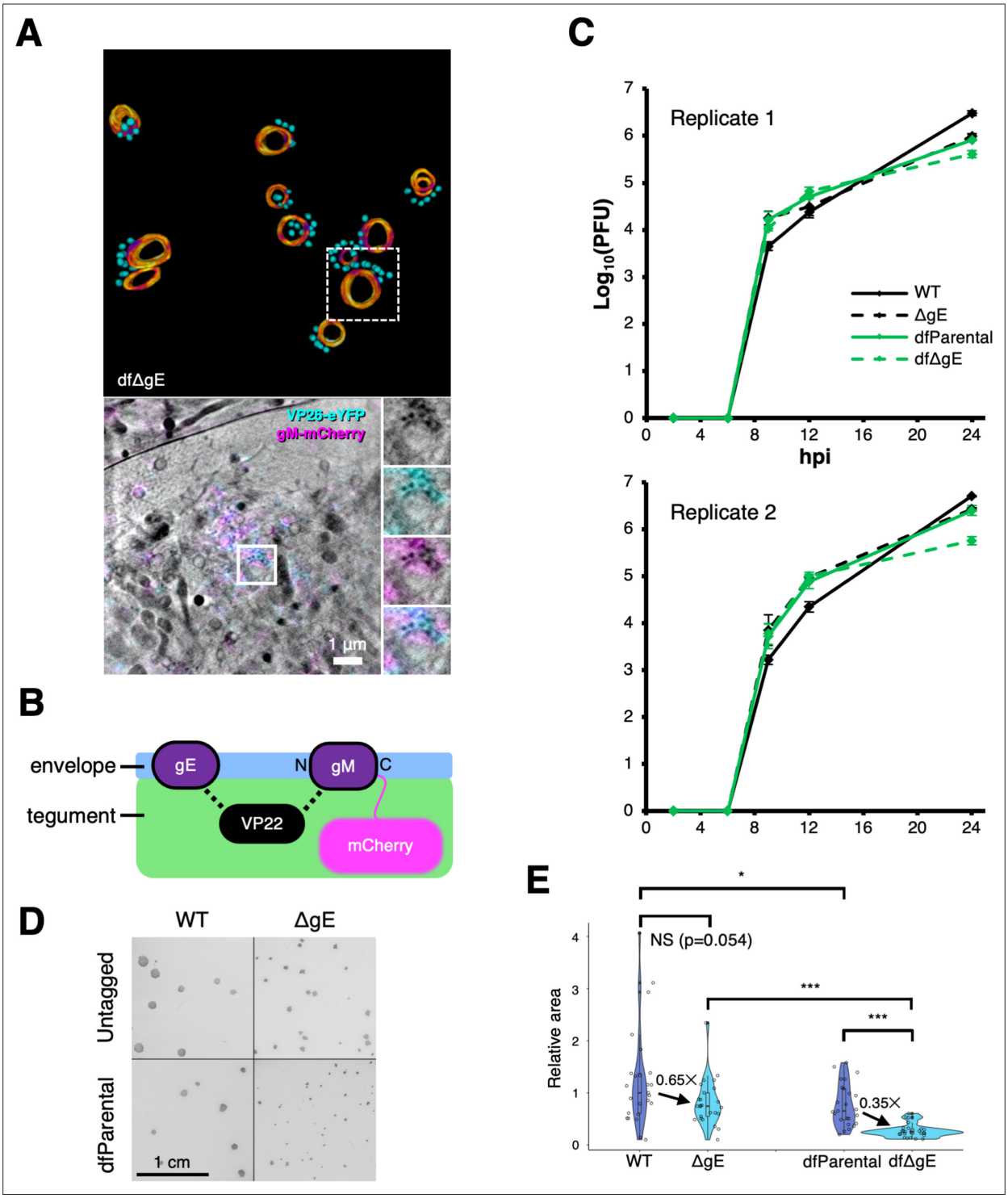

Figure 8—figure supplement 2. Impact of the gM-mCherry conjugation on the ΔgE virus. (**A**) Numerous stalled envelopment events were observed for the dual fluorescent ΔgE virus (labelled dfΔgE only in this figure). Scale bars = 1 μm. (**B**) Schematic of known interactions between tegument component VP22 and envelope components gE and gM. (**C**) Neither absence of gE expression nor gM-mCherry tagging dramatically altered the replication kinetics of HSV-1 mutants. U2OS cells were infected at MOI = 2 with virus over a 24 hr period and were treated with citric acid at the 1 hr timepoint to deactivate residual input viruses. Two biological replicates were performed, with two technical repeats for each timepoint. dfParental and dfΔgE data are the same as those shown in ***Figure 2A*** and ***Figure 2—figure supplement 1***. Error bars show mean ± SD. (**D**) U2OS cells were infected with indicated viruses, were covered in media containing 0.6% (v/v) CMC after 1 hr, and plaques were fixed and stained 72 hpi (N=25 for each recombinant virus). Scale bars = 1 cm. (**E**) Relative plaque size was calculated for each virus. Mann-Whitney U tests were used to assess the significance of differences. P-value thresholds: <0.05 (*), <0.005 (**), and <0.0005 (***). NS, no significance.

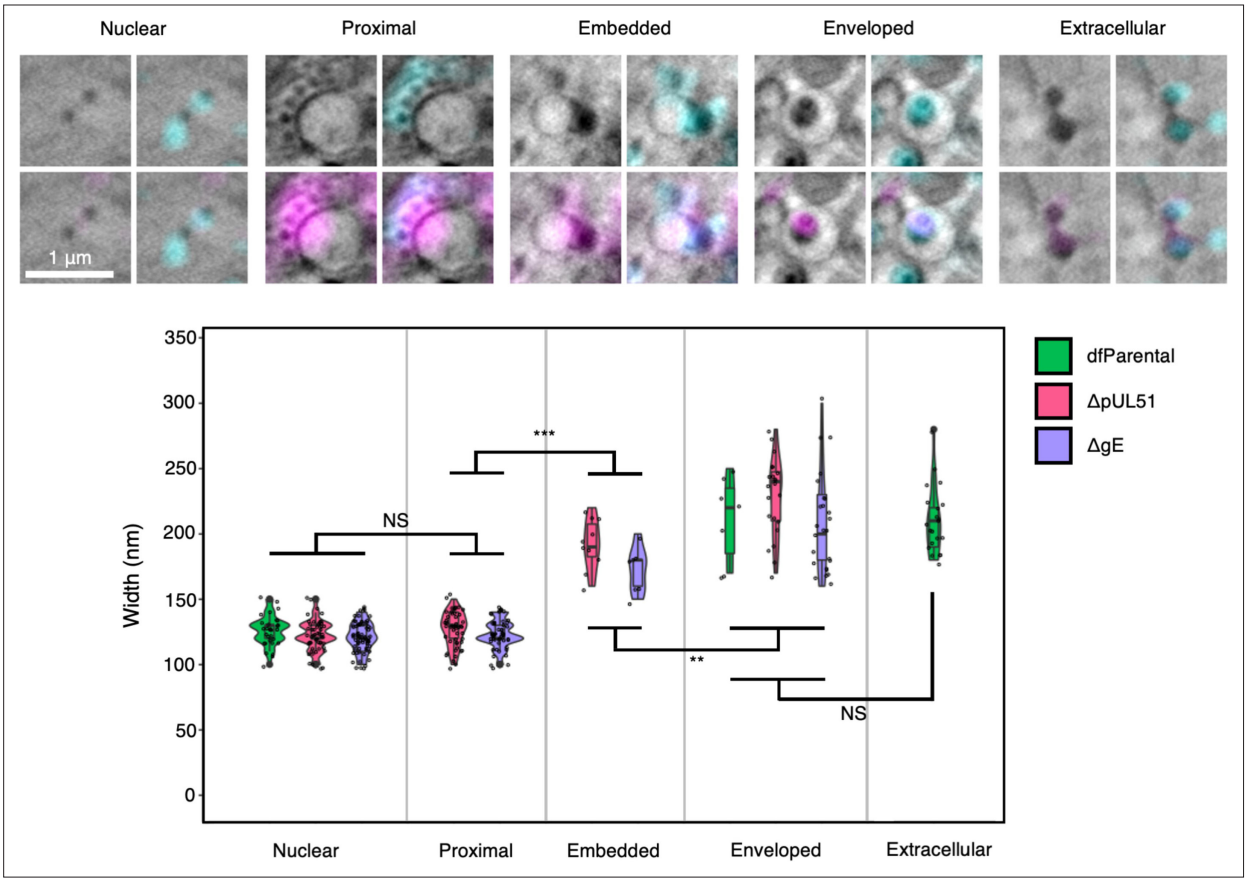

Figure 9. Cryo-soft-X-ray tomography (CryoSXT) resolved differences in the widths of virus assembly intermediates. U2OS cells were infected at MOI = 2 for 16 hr. Widths of virus particles at different stages of assembly were measured for the dfParental, ΔpUL51, and ΔgE viruses. See ***Table 1*** for values. Mann-Whitney *U* tests were used to assess the significance of differences. No significant differences in width were observed between virus musctants at the same stage of assembly, except for enveloped ΔgE (N=25) and ΔpUL51 (N=22) virus assembly intermediates (*p*-value = 0.0285). P-value thresholds: <0.05 (*), <0.005 (**), and <0.0005 (***). NS, no significance. Scale bars = 1 µm.